catalysts

MDPI

Review

The Mechanism of Adsorption, Diffusion, and Photocatalytic Reaction of Organic Molecules on TiO_2 Revealed by Means of On-Site Scanning Tunneling Microscopy Observations

Peipei Huo *, Parveen Kumar and Bo Liu *

Laboratory of Functional Molecules and Materials, School of Physics and Optoelectronic Engineering, Shandong University of Technology, Xincun West Road 266, Zibo 255000, China; kumar@sdut.edu.cn

* Correspondence: peipeihuo@sdut.edu.cn (P.H.); liub@sdut.edu.cn (B.L.); Tel.: +86-05332787883 (P.H.); +86-05332783909 (B.L.)

Received: 13 November 2018; Accepted: 29 November 2018; Published: 4 December 2018

Abstract: The interaction of organic molecules and titanium dioxide (TiO_2) plays a crucial role in many industry-oriented applications and an understanding of its mechanism can be helpful for the improvement of catalytic efficiency of TiO_2. Scanning tunneling microscopy (STM) has been proved to be a powerful tool in characterizing reaction pathways due to its ability in providing on-site images during the catalytic process. Over the past two decades, many research interests have been focused on the elementary reaction steps, such as adsorption, diffusion, and photocatalytic reaction, occurring between organic molecules and model TiO_2 surfaces. This review collects the recent studies where STM was utilized to study the interaction of TiO_2 with three classes of representative organic molecules, i.e., alcohols, carboxylic acids, and aromatic compounds. STM can provide direct evidence for the adsorption configuration, diffusion route, and photocatalytic pathway. In addition, the combination of STM with other techniques, including photoemission spectroscopy (PES), temperature programmed desorption (TPD), and density functional theory (DFT), have been discussed for more insights related to organic molecules-TiO_2 interaction.

Keywords: STM; TiO_2; photochemistry; atomic resolution

1. Introduction

Over the last decades, the interest in titanium dioxide (TiO_2)-based materials has been increased enormously since Fujishima and Honda's first reported the water-splitting ability of illuminated TiO_2 [1]. TiO_2 has been shown to be useful for the heterogeneous photo-catalysis, dye-sensitized solar cells, water and air purification, deterioration of bacteria, inactivation of cancer cells and gas, sensor, and anti-corrosive coatings [1–17]. Therefore, TiO_2 has been an important target for industry-oriented applications [2–5]. In the research on TiO_2-based materials, researchers mainly focus on the preparation of novel materials or increasing the final photocatalytic activities. It has been reported that a nanostructured TiO_2 nanorod supported on various foreign substrates may enhance TiO_2's light harvesting capacity [18]. Metals, such as Pt, Au, and Cu, supported on TiO_2 can work as photocatalysts for reactions, such as methyl formate decomposition and CO_2 reduction [19,20]. However, the reports focusing mainly on the mechanism, such as an activation site or reaction pathway, in the photocatalytic process are scarce. Conventionally, the currently widely accepted working mechanism of nanostructured TiO_2-based photocatalytic materials has been developed, first of all, by characterizing the crystal structure and morphology of catalysts using X-ray diffraction (XRD), field emission scanning electron microscopy (FESEM), and corresponding energy-dispersive X-ray

spectroscopy (EDS) [21,22]. The typical diffraction peaks displayed in XRD describe the crystal phase within the TiO_2 catalysts. FESEM is especially insightful in characterizing the TiO_2 catalysts' geometry highest to the nano scale. After obtaining this information, a number of molecular spectroscopies were utilized to characterize the photo-excited charge carriers, such as electrons and holes [23–26]. As a result, the process of active radical generation, electron-hole pair recombination, and subsequent photocatalytic oxidation involved with those photo-induced charge carriers were analyzed in detail. Then, the mechanism has been generally obtained through analyzing the initial and final state of the reactant on the average molecular level, where the direct evidence, such as on-site images tracking one specific molecule's reaction route, is absent. The more fundamental mechanism obtained through the atomic level characterization tool is scarce. Therefore, it is highly important to understand the on-site mechanism in the catalytic process, because the knowledge can be utilized to optimize the preparation of catalytic materials, which in turn maximizes the catalytic efficiency. The existence of a series of surface science tools represented by scanning tunneling microscopy (STM) provides a useful solution to this problem. The images obtained by STM provide strong evidence of a reaction's pathway because it is directly observed using on-site images with atomic resolution. Furthermore, TiO_2 is generally preferred as a model transition metal oxide for fundamental studies due to the fact that it can be easily prepared and reduced under ultrahigh vacuum (UHV) conditions [27–33], which makes the crystals conduct and thereby enabling its use in several different surface science techniques. An Au supported-on TiO_2(110) system can be characterized by STM as well [34].

The fundamental working mechanisms of photo-catalysis on semiconductors generally contains several elemental steps, such as (1) adsorption of reactants and diffusion of the adsorbed reactants to the active sites, as in common heterogeneous catalysis; (2) absorption of light and excitation of the electron-hole pairs, where the photoactive semiconductor acts as the light absorber; (3) charge transport, separation, and transfer to the absorbed reactants, where the charge trapping might play a role in decreasing the following electron or hole mediated reaction; and (4) reaction of the reactants and desorption of the products. The on-site knowledge of each catalytic process with atomic resolution is necessary for optimizing the catalytic results.

The optimization of catalysts with advancing properties underlies the need for detailed information, including the bonding of adsorbates on the substrate, particle size, structure, composition, and spatial distribution. In applied catalytic studies, the catalysts are simulated for industrial use by varying the parameters, such as quantity of reactant, temperature, pH, calcination, and reduction procedures, etc., which are unable to provide the desired characterization of supported catalysts at an atomic scale. On the other hand, a surface science approach can provide desired nanoscale information in which the heterogeneous catalysis is generally simplified by either well-defined single crystals of the supported phase and particles or films of that phase on flat or spherical model supports. A detailed understanding of the photo-catalytic process is probably only possible to achieve through fundamental surface science studies of model catalysts. Among surface science characterization techniques, STM has been proved to be a powerful tool in studying materials' surfaces at an atomic scale. STM applies the tunneling effect known for the quantum mechanics and the surface geometric or electrical structure that can be imaged by analyzing the tunneling current in the atoms on solid surfaces. According to quantum mechanics, the wave feature of the particle makes it tunnel through a classically forbidden region. The electrons are not totally confined within the metallic surface, i.e., the density of the electron state does not drop off to zero on the surface boundary. Beyond a metallic surface, the density of the state decays exponentially within a distance of ~1 nm. By bringing an extremely sharpened tip into close proximity of the conducting sample, the electronic wave function of the tip and sample surface tend to overlap. Upon applying a tunneling voltage, the electrons tunnel through the tip-surface electrodes as the tip-sample distance is sufficiently small (below a few nm), leading to a measurable tunneling current. With the tip-sample junction in this state, the tip is then scanned across the surface in a raster pattern. The most common operating mode is the "constant current mode", where a feedback loop is used to regulate the tip height to keep the current constant. The STM image produced in this

way shows contours of constant gap resistance and always reflects the convolution of the geometric and electronic structure of the surface, but in some cases, one of the two effects completely dominate the contrast of the image. For example, STM images of metal surfaces can often be interpreted as topographic maps of the surface, whereas STM images of a metal oxide, such as the rutile TiO_2(110) surface, are dominated by the electronic structure. The tunneling current exponentially depends on the tip-sample distance where every 0.1 nm change in distance leads to a change in the tunneling current by one magnitude.

Surface science approaches represented by STM have been intensively applied in order to resolve the catalytic mechanism occurring on the TiO_2 surface to find the parameters in each single step, such as adsorption, diffusion, and photo-reaction. The specific behavior of the adsorption, diffusion, and photo-reaction mainly depends on the molecular structure. Therefore, this review elaborates each of the three processes with three different classes of representative organic molecules, such as alcohols, carboxylic acids, and aromatic compounds. This review aims to collect the studies where STM has been used as the main tool to characterize on-site images. The functions of STM have been elaborated in three sections. Section 2 mainly focuses on the adsorption structure resulted when a TiO_2 surface is exposed to organic molecules. Section 3 elaborates the diffusion occurring at the TiO_2 surface, since STM can track a dynamic process with its fast scanning ability, and Section 4 reveals the catalytic pathways in a photo-reaction.

2. Adsorption Structure

TiO_2 has two prototypical surfaces, i.e., rutile TiO_2(110)-(1 × 1) surface and anatase TiO_2(101) surface. Rutile TiO_2(110)-(1 × 1) surface consists of alternating rows of fivefold-coordinated Ti atoms (5f-Ti) and protruding, twofold-coordinated bridging oxygen (O_{br}) atoms. The reduction of TiO_2(110) crystal results in a surface defect in the form of O_{br} vacancies (O_{vac}). The empty-state STM images of the TiO_2(110) surface are primarily decided by electronic effects, resulting in a reversed contrast. So, bright rows indicate the Ti troughs, whereas geometrically protruding O_{br} rows are dark. The O_{vac}s appear as faint bright spots on the dark O_{br} rows. Contrary to the rutile TiO_2(110)-(1 × 1) surface, there is no O_{vac} on the anatase TiO_2(101) surface, so no bond cleavage dissociative adsorption is expected. Since there is no O_{vac} in the natural atmosphere, the result of the catalytic pathway revealed on this surface resembles the real catalytic system in a higher degree.

Many heterogeneous catalytic reactions are initiated by the adsorption of organic molecules. In order to resolve the catalytic mechanism occurring on the surfaces of the catalyst, the surface science approach has been applied to find the parameters, such as the adsorption site and the adsorption structure.

Alcohols are good prototypical molecules to study the photocatalytic reaction of organic molecules with TiO_2. Hansen et al. studied the adsorption state of ethanol (EtOH) on rutile TiO_2(110), where two structures of molecular and dissociated adsorbates have been clearly characterized using STM. As shown in Figure 1, at 130 K, one type of adsorbates was found exactly on top of 5f-Ti sites, whereas the other was at O_{br} positions. Except for the adsorption position, the two types of adsorbates can also be discernible in the STM by their different apparent heights (i.e., brightness). In the Ti trough, the brighter adsorbate was ~0.7 Å higher than the smaller adsorbate and the adsorbates centered on the O_{br} rows had the same STM height as the small adsorbates. The less bright adsorbates in the Ti troughs were assigned to ethoxide groups (EtO_{Ti}) and the brighter adsorbates to molecularly adsorbed EtOH ($EtOH_{Ti}$). The adsorbates bound at the O_{br} rows with STM heights of ~2.0 Å were assigned to ethoxide groups (EtO_{br}) bound at O_{br} vacancies [35]. The assignment of contrast difference to different adsorption configuration set a good example for STM image analysis. For example, in the study where a saturation coverage of 0.5 monolayer (ML) monoethanolamine (MEA, $HO(CH_2)_2NH_2$) adsorbed on the rutile TiO_2(110) surface presents a configuration, where O of the OH group and N of the NH_2 group bound to neighboring 5f-Ti sites in the Ti troughs. However, there is no discernible contrast difference between dissociated and molecular adsorption in the STM images, which might be due to

changes in coverage, compared with the results of Hansen et al. [36]. Zhang et al. studied methanol (CH_3OH) adsorption on the rutile TiO_2(110) surface by STM and found that CH_3OH dissociatively adsorbed at the O_{vac} sites, with O–H bond cleavage and one hydroxyl formation at neighboring O_{br} sites, similar to EtOH dissociation [37].

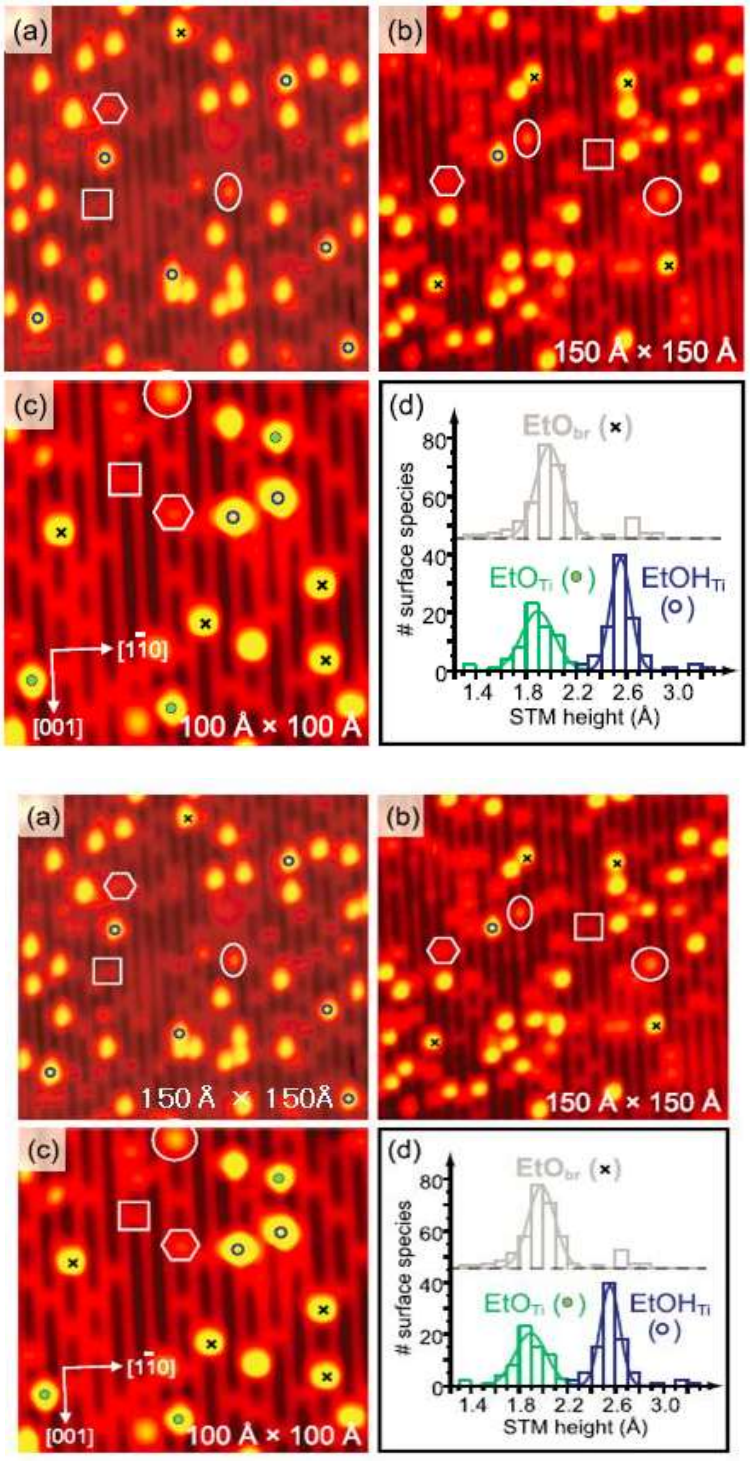

Figure 1. STM images obtained after EtOH exposure onto TiO_2(110): (**a**–**c**) EtO_{br} are indicated by a black cross, EtO_{Ti} by a green solid dot, $EtOH_{Ti}$ by a hollow blue circle. Other symbols indicate O_{vac} (square), H adatom (hexagon), H adatom pair (square), and water (ellipse), respectively. (**d**) STM height histograms of the three adsorbates (Reprinted figure with permission from [35] Copyright (2011) by the American Physical Society).

A lot of research interests are dedicated to the adsorption structure of molecules with a carboxylic acid group. One of the photocatalytic applications of TiO_2 is in the dye-sensitized solar cells, which often include interfaces with carboxylate-anchored organic molecules [38]. Trimethylacetic acid (TMAA) is one such conventional carboxylic acid probe with two adsorption channels, which can adsorb dissociatively with deprotonation in the acid group, leading to carboxylate species and trimethyl acetate (TMA) bridge-binding at two Ti sites. The second adsorption geometry is O_{vac} sites bind to one O atom in TMA, while the other O atom in TMAA binds to another Ti site [39,40]. The interactions of formic acid and acetic acid with the rutile TiO_2(110) surface have been investigated and found to have quite a different adsorption structure. With a 10 mM solution dipping on the surface, formic acid bound with the surface in two different configurations and formed overlayer had no apparent ordered structure. On the other hand, acetic acid constitutes a well-ordered acetate overlayer with a (2 × 1) periodicity, analogous to that exposed to vapor [41]. Formic acid adsorbed on anatase TiO_2(001) in the form of formate and were imaged as protrusions adsorbed at under-coordinated Ti sites in the added rows. Oddly, no such formate species adsorption was found in the trenches where under-coordinated Ti atoms were likely to be exposed [42]. The adsorption of acetic acid on anatase TiO_2(101) has been also investigated with STM and found that at low coverage, acetic acid dissociatively adsorbed in the form of bidentate binding adsorbate. Whereas, at 420 K, a saturated coverage displays a partially ordered superstructure with two domains of which the periodicity was found to be (2 × 1), as a result of a bidentate binding geometry of the acetate to two adjacent Ti sites along the [010] direction [43]. Pang et al. utilized STM and noncontact atomic force microscopy (NC-AFM) to study methyl phosphonic acid adsorption on rutile TiO_2(110)-(1 × 1) and revealed that, at low coverage, methyl phosphonic acid preferably adsorbed on the 5f-Ti troughs. However, on rising the adsorbate coverage to 0.5 ML, phosphonic acid was deprotonated to produce phosphonate and STM images displayed an ordered (2 × 1) overlayer, which can be attributed to the phosphonate bridging conformation across two neighboring 5f-Ti atoms in the [001] direction [44].

Aromatic compounds are another representative class of organic molecules, in which the aromatic ring often plays an important role in the interaction with TiO_2 [41]. The interaction of benzoic acid on the TiO_2(110) surface was observed as dissociative adsorption, leading to benzoate and hydroxyl groups' formation. The adsorption of benzoate formed an ordered pseudo-(2 × 1) overlayer, which can be explained by bonding through the carboxyl group with Ti^{4+} cations. Dimer rows along the [001] direction were observed probably due to attractive interactions between aromatic rings of the benzoates [45]. Motivated by the function that terephthalic acid (TPA) molecules performed in some of the metal-organic frameworks, Prauzner-Bechcicki et al. investigated the adsorption structure of TPA on rutile TiO_2(110)-(1 × 1) and the study revealed that one ML of TPA bound to the surface with a bidentate pattern forms dimer rows in the [001] direction due to tilting and rotating of adjacent TPA molecules. In addition, the molecules were inclined to display an upward growth tendency with a –COOH group facing the vacuum [46,47]. Iwasawa et al. have successfully visualized the adsorption structure of pyridine and its derivatives on rutile TiO_2(110)-(1 × 1) surface by using STM. Individual pyridine and 2,6-dimethylpyridine (2,6-DMP) molecules weakly adsorbed on the surface and desorbed near RT without chemical bond formation [48].

The molecular structure itself can affect the adsorption configuration to a great deal. Besides this, adsorption geometries often depend on several other factors, such as the coverage, interactions between adsorbates, and reconstruction of the substrate. Some of the examples have been discussed here to study these factors in detail. The interaction of perylene on the TiO_2(110)-(1 × 1) surface at different surface coverages was studied and found that the coverage has a determining influence on the adsorption configuration. However, at the submonolayer, the perylene displayed itself as elongated protrusion adsorbed on the Ti trough and the distribution did not reflect any intermolecular interaction. Furthermore, when the coverage increased to the limit of the first layer, an ordered compact domain of perylene was observed due to side-to-side molecular attraction [49]. Perylenetetracarboxylic-diimide, (PTCDI) molecules adsorbed in the form of lying on their long edges, tilted by ~35° with respect

to the surface due to steric repulsion with the first layer deposition. A strong π-π coupling between neighboring molecules determines an aggregation into islands corresponding to a (1 × 5) commensurate phase [50]. Adsorption of anthracene and 4-bromobiphenyl on a TiO_2 rutile (110) surface have been studied by STM, which showed that both molecules can adsorb on the TiO_2 surface by forming periodic patterns with every single molecule oriented along the 5f-Ti row. The observed surface arrangement suggests an attractive interaction between the anthracene molecules across the rows whereas a strikingly different alignment of bromobipheneyl molecules indicates repulsive interaction [51]. Copper phthalocyanine (CuPc) on reconstructed cross-linked rutile TiO_2(110)-(1 × 2) was investigated and found that at low coverages, CuPc sparsely lay flat at the link sites and tilted in troughs between [001] rows. However, as the coverage increased, CuPc molecules were trapped in the rectangular surface cells separated by the oxygen columns along the [001] direction and the cross-link rows [52]. Most adsorbates can present themselves in multiple adsorption geometries, with preference depending on thermodynamics. One state can be automatically converted to another in an energetically allowed condition. Such a conversion process occurs when formaldehyde (HCHO) molecules adsorb on the rutile TiO_2(110) surface. There are two types of protrusions of HCHO molecules, one centered at 5f-Ti rows correlating with the monodentate adsorption binding with the O-(5f-Ti) bond and the other centered at O_{br} rows as a bidentate adsorption with both O-(5f-Ti) and C-O_{br} bonds. The former can spontaneously be converted to the latter, indicating the energetically more preferable bidentate adsorption. Density functional theory (DFT) calculations provide energy barriers of 0.28 and 0.75 eV for the conversion from monodentate to bidentate adsorption and for the reversed process, respectively, thereby confirming the more favorable bidentate adsorption [53].

3. Diffusion

Whether a molecule is stabilized or mobile on the substrate surface depends on the balance between adsorbate-substrate and inter-adsorbate interactions. If the inter-adsorbate attraction surpasses the adsorbate-substrate interaction and overtakes the molecular diffusion barrier, the adsorbate molecule would be fairly mobile [52]. Surface diffusion is generally important in interfacial processes, such as self-assembly or heterogeneous catalysis.

Hansen et al. tracked the dynamics of three adsorbates by recording time-lapsed STM movies (Figure 2) and this method was used to confirm the assignment of three adsorbates. The EtOH molecular adsorbate was observed to diffuse along the Ti trough, and then reached to a 5f-Ti site close to O_{vac} and jumped into the O_{vac} where it got trapped:

$$EtOH_{Ti} + O_{vac} \rightarrow EtO_{br} + OH_{br} \text{ (H adatom)}$$

Simultaneously, the apparent height of the adsorbate decreased by ~0.6 Å to ~2.0 Å and this event can be explained as an $EtOH_{Ti}$ molecule that diffuses along the Ti trough and dissociates at the O_{vac} via O–H bond cleavage. The resulting EtO_{br} and H adatom were located on the neighboring O_{br} sites. The species assigned to EtO_{Ti} was immobile at ~191 K. However, the significantly different mobility of the three species provides further evidence of the assignments [35]. Likewise, the observation that molecular CH_3OH can diffuse along the 5f-Ti rows at RT confirms the assignment that CH_3OH does not dissociate at 5f-Ti sites [37]. On the same surface, EtOH diffusion in both directions of parallel and perpendicular to the rows of O_{br} and Ti atoms were imaged. Contrary to the diffusion along the Ti rows (Figure 3), the diffusion of EtOH perpendicular to the rows of Ti atoms was mediated by H adatom species. Additionally, the diffusion of H adatom species across the Ti rows, mediated by EtOH molecules, was rarely observed [54]. Probably due to the small molecular weight, the diffusion process of an organic molecule with one or two carbon atoms is fairly easy to observe. Consecutive STM images were used to reveal the reaction pathway of ethylene from HCHO adsorption. HCHO preferably adsorbed on the O_{vac} sites, forming O_{vac}-bound species and the intact HCHO diffused along

the Ti row and then diffused to nearby O_{vac} sites upon C–O bond dissociation. Afterward, this HCHO coupled with another HCHO located across the Ti row and desorbed as an ethylene molecule [55].

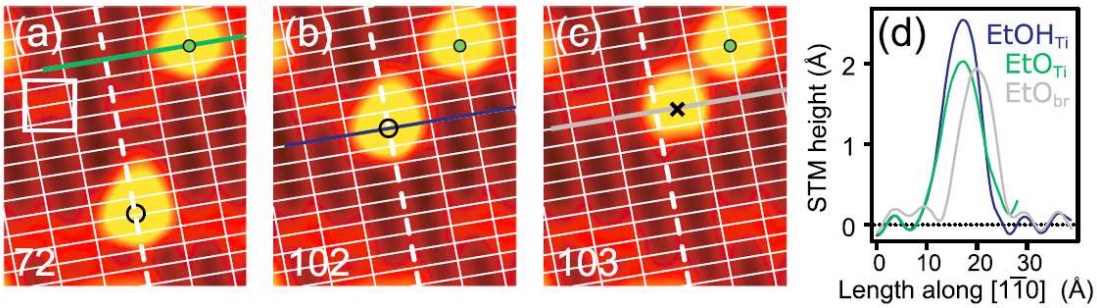

Figure 2. Consecutive STM images recording the diffusion and dissociation of a single EtOH molecule. (**a**–**c**) EtOH (indicated by a black open circle) diffuses along the Ti trough, gets trapped at O_{vac}, leading to EtO_{br}. Other symbols have the same indications as in Figure 1. (**d**) STM height profiles along the lines indicated in (**a**–**c**) (Reprinted figure with permission from [35] Copyright (2011) by the American Physical Society).

TMA diffusion tends to be forbidden at RT due to its chemical bond with the surface. There were calculations indicating that the more common bridging configuration of TMA at the Ti rows was slightly less favorable than that bound at the O_{vac} site. TMAA molecules displayed themselves initially in a mobile physisorbed state, whereas the diffusion of the chemisorbed TMA species was significantly slow at RT with a calculated barrier of 1.09 eV [40]. On the contrary to the surface of (1 × 1) TiO_2(110) where TMAA dissociated, TMAA diffuses readily along the troughs on (1 × 2) reconstructed TiO_2(110) at low coverages, indicating that TMAA adsorbs in a molecular state. At RT, TMAA species was observed migrating back and forth along troughs at the low coverages (<0.05 ML) when it was isolated [56].

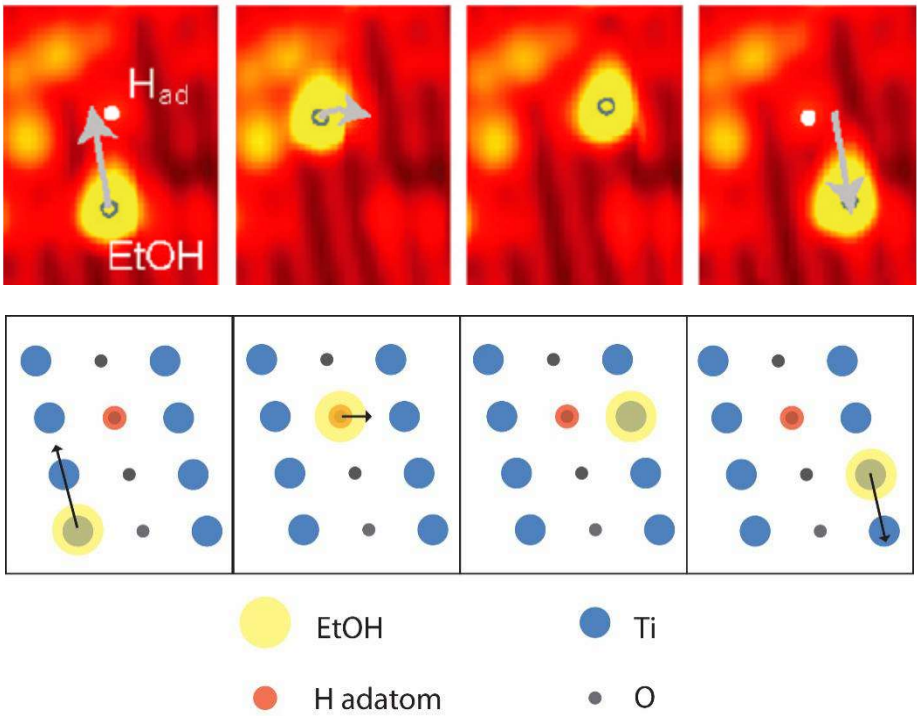

Figure 3. STM snapshots recording EtOH diffusion along and perpendicular Ti row (**upper row**) (Reprinted figure with permission from [54] Copyright (2012) by the American Chemical Society). Corresponding ball model scheme (**lower row**).

It was indicated that the barrier for surface diffusion depends on the interaction of adsorbates with the substrate. For example, pyridine does not form a strong chemical bond with rutile TiO_2(110), therefore a fast diffusion occurs in such an adsorbate-substrate scenario. At RT, the adsorbates can move so fast that it cannot be imaged with a whole shape since the raster scanning motion around a 2500 $Å^2$ area takes ~5 s. Iwasawa et al. attributed their fragmented shapes of the molecular image to the migration of adsorbed pyridine molecules. While in the case of 2,6-DMP adsorption, such fragmented shapes of adsorbates were not observed whereas a short distance migration of minority of molecules in the [001] direction was found in the consecutive scanned images within the same area. Since most molecules stayed in the same position, therefore, it can be concluded that the diffusion of 2,6-DMP is much slower than pyridine [48]. Except for adsorbate-substrate interaction, coverage is another factor affecting the diffusion behavior of aromatic compounds, especially when the adsorbates are densely-packed. The single molecule vacancy diffusion was observed within the TPA ML. Such migration proceeds along the grain boundary through a series of consecutive scans in the same area indicates a rather a low barrier for surface diffusion of TPA molecules in the ML along the [001] substrate direction [46]. Osgood et al. observed some poorly defined features of anthracene in a high-resolution image, which were not because of instrumental or stability artifact. In the densely-packed area, the mobility was restricted and images were well-resolved. Whereas in the poorly-populated area, the molecules were fairly mobile in the [001] direction due to thermal oscillation, thus the whole shape of the molecule has not been obtained [51]. Jensen et al. demonstrated butyrophenone adsorbed as an intact molecule at the Ti row and weak binding made it diffuse freely along the Ti rows even at 55 K. This diffusion was confined in a one-dimensional potential well formed by strongly bound butyrophenone-O complexes [57].

Since diffusion is an essential elemental step in a TiO_2 catalyzed reaction of organic molecules, but there are many cases where adsorption studies outnumbered the diffusion and the reason should be because adsorption can be easily observed by STM no matter whether it is a strong or weak adsorption configuration. However, even in the studies where diffusion has been labeled as the main research interest, adsorption is always the pre-study or supplementary study. Moreover, when the diffusion occurs on a time scale faster than STM scanning speed, it appears only some fragmented feature that could be captured by the STM image. Notably, we should not overlook the role of STM in characterizing the diffusion process.

4. Photo-Catalytic Reaction

Since TiO_2 is a semiconductor in nature and photocatalytic reactive, nearly every STM investigations involved with TiO_2 are oriented toward the destination of gaining a more insightful understanding about its photo-catalytic reactivity. Weakly adsorbed $EtOH_{Ti}$ and EtO_{Ti} species in the Ti troughs of TiO_2(110) decompose rapidly to CH_3CHO when exposed to UV light, even in the absence of O_2. On the contrary, EtOH species adsorb dissociatively in the O_{vac} (EtO_{br}) and react slowly along [111]-type step edges. Regular 5f-Ti sites are the most important sites for the photo-catalytic conversion of alcohols into their corresponding aldehydes/ketones on rutile TiO_2(110) [58]. The ethanol reaction scheme has been summarized in Scheme 1 as a result of STM investigation of ethanol-rutile TiO_2(110) interactions. Idriss et al. studied the photocatalytic reaction of ethanol over the anatase TiO_2(101) surface and found that upon UV illumination with the atmosphere of oxygen, some ethanol disappeared whereas large protrusions arranged in a (1 × 2) pattern formed along the [010] direction, which was assigned as carboxylate adsorb in a bidentate manner. Upon excitation in the presence of O_2, the main product was acetaldehyde [59].

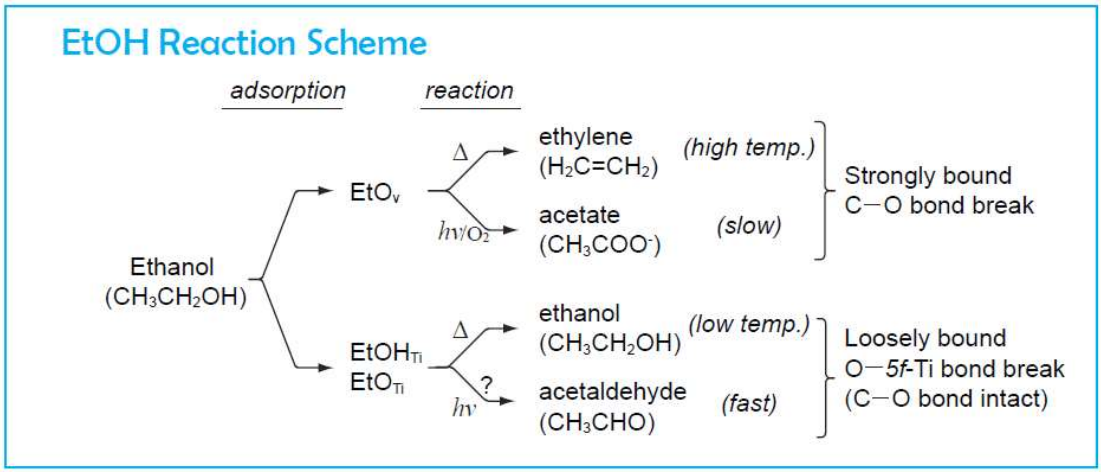

Scheme 1. EtOH reaction scheme.

Likewise, CH_3OH, which is a good probe molecule of alcohol, can be potentially applied in photocatalytic selective oxidation, environmental photocatalysis, and photocatalytic reforming reaction. Zhou et al. investigated the CH_3OH photo-oxidation on TiO_2(110). After 10 min of UV (<400 nm) irradiation, most of the Ti^{4+} bound molecular CH_3OH species became elongated and these elongated species were split into two parts by pulling them with an STM tip. One dim protrusion left on the O_{br} site was assigned to be an OH_{br} group. Thus, the UV irradiation was proved to make the CH_3OH molecule dissociate. Similar STM experiments using light irradiation (>400 nm) have also been carried out and gained no evidence for CH_3OH dissociation, suggesting that the dissociation of CH_3OH was a substrate-mediated photocatalytic process [60]. Later, the same research group observed a complete photocatalytic process for a single CH_3OH molecule by recording STM images of the same small area at different UV irradiation time intervals. Thus, the photodecomposition of CH_3OH into HCHO and OHs on TiO_2(110) have been directly visualized [61]. HCHO and methyl formate ($HCOOCH_3$) were produced from the photo-oxidation of CH_3OH. After production of HCHO, transient HCO was made photochemically. In the next step, the HCO reacts with a residual methoxy group to yield $HCOOCH_3$. There is a pre-requisite for these photo-oxidation steps to occur because surface and near-surface defects are needed to be healed [62]. The photoactivity of isolated CH_3OH adsorbed on the anatase TiO_2(101) surface showed a negligible photoactivity. Two pathways of CH_3OH activation were explained by combining STM with other characterization techniques, such as temperature programmed desorption (TPD) and DFT (Figure 4). First, the methoxy groups were produced via reaction of CH_3OH with coadsorbed O_2 molecules or terminal OH groups, leading to HCHO formation upon UV illumination. On increasing the CH_3OH coverage to above 0.5 ML, activation occurs, leading to the formation of methyl formate. Partial dissociation of CH_3OH to methoxy is the key step in both the processes [63]. The CH_3OH reaction scheme has been summarized in Scheme 2 and by comparing reaction schemes of EtOH and CH_3OH, it can be concluded that molecular or dissociatively adsorbed species bound to Ti sites are photo-active, which can lead to the aldehyde product. However, with EtOH having two C atoms, a C=C structure forms in the O_{vac}-bound species, which can subsequently lead to CH_3COOH whereas the process of C=C formation cannot be observed with CH_3OH. One of the oxidized products of CH_3OH is formic acid (HCOOH), which can in principle be further photo-oxidized. However, there is no report on HCOOH photo-oxidation on a TiO_2(110) surface, probably because the band gap of the surface is as big as the bulk one. Iwasawa et al. reported that on the TiO_2(001) surface, HCOOH adsorbates changed into OH groups upon UV irradiation and with the O_2 atmosphere. The study proved that the photon threshold energy of a photochemical material can also be determined by a smaller surface state, compared with the bigger bulk band gap [64].

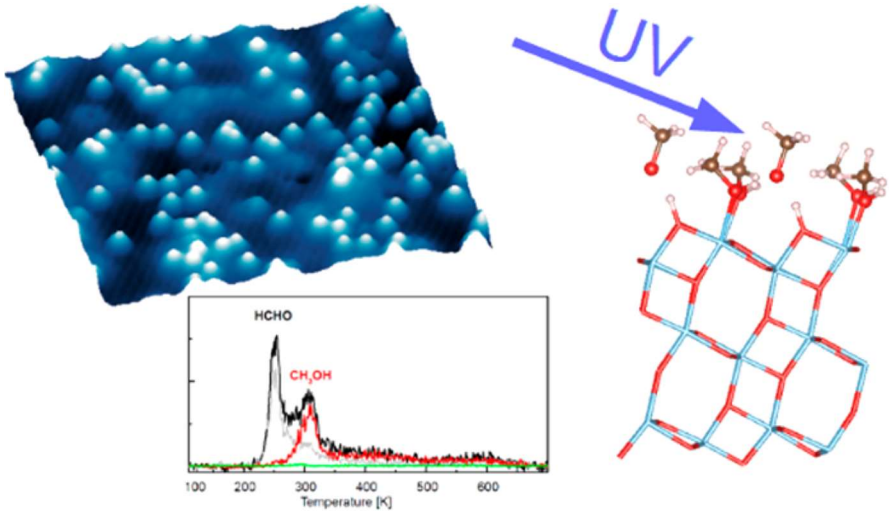

Figure 4. 3D STM image, ball-bond model applied in DFT, and TPD results relevant to CH_3OH photocatalysis on anatase TiO_2(101) (Reprinted figure with permission from [63] Copyright (2017) by the American Chemical Society).

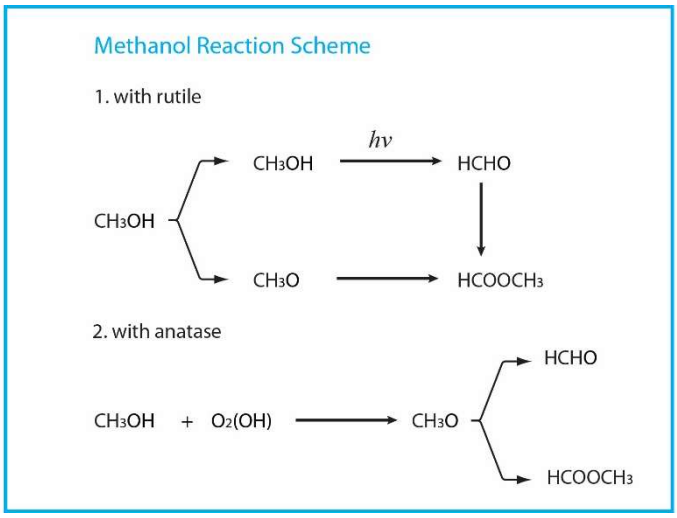

Scheme 2. CH_3OH reaction scheme.

Since TMAA molecule dissociatively adsorbs at the rutile TiO_2(110) surface, the photo-reactivity actually depends on the dissociation form of TMAA, which generates TMA and binds at Ti sites undergoing hole-mediated photolysis upon UV illumination, resulting in the formation of CO_2 and tert-butyl radical [65,66]. On the other hand, TMA species bound at O_{vac} sites are completely inactive toward UV light [67]. Lyubinetsky et al. observed a decreasing reactivity of TMA on TiO_2(110) with coverage and this hindering effect originated from the accumulated OH_{br} generated when the parent TMAA dissociatively adsorbed on TiO_2(110). This effect was confirmed by the fact that OH_{br} groups stemming from H_2O dissociating at O_{vac} sites exert an analogous inhibiting influence on TMA photolysis. Considering the function of OH_{br} species as trap sites for photogenerated electrons, which attract and neutralize photogenerated holes, it is fairly reasonable to conclude the negative influence on photochemistry [68]. The photoreaction of TMAA on an isolated TiO_2 nanocrystal grown in situ on Au(111) in an UHV chamber was studied by Osgood et al. by analyzing STM images and found that the atomic structure of the dominant type of TiO_2 nanocrystals exerted a mismatch between rutile and gold lattice parameters. The normalized TMAA photodesorption quantum efficiency from Au-supported TiO_2 nanocrystals was found to be ~4 times lower compared to the same reaction on the rutile TiO_2(110) surface due to the lower fraction of light adsorbed in the nanocrystals [69].

Photochemistry of various aromatic compounds on TiO_2 has been also investigated. For example, benzoic acid deprotonated to benzoate, which was intact under UV illumination for several hours. The stability of benzoate under illumination demonstrates the importance of substituents on the stability of the molecular layer [70]. Butyrophenone thermally reacted with oxygen adatoms on oxidized TiO_2 to create a photoactive butyrophenone-O complex. STM experiments demonstrated that 22 bigger, oval-shaped butyrophenone-O complexes changed to 22 smaller, "L"-shaped benzoate species, indicating a 1-to-1 correlation between the two species. Additionally, the benzoate produced was found at nearly the same site as the original butyrophenone-O complex, suggesting that the photoproduct was rapidly trapped. A controlled experiment indicated oxygen adatoms were necessary for photolysis from butyrophenone to benzoate, since on reduced TiO_2, there was no change observed in the STM images before and after UV illumination [71].

5. Challenges and Outlook

The common traits in the behavior of adsorption, diffusion, and photocatalytic reaction are summarized in Table 1, addressing the interaction of organic molecules with different TiO_2 surfaces. The studies were mainly performed by STM in combination with complementary experimental techniques and computational methods, such as PES, TPD, and DFT calculations. The STM provides a unique ability to follow individual processes on the surfaces and allows to follow the diffusion and reaction of a single molecule with very high spatial and temporal resolution. Even though much applied research on TiO_2 is undertaken to study photo-assisted degradation of organic molecules, the number of surface science studies is, however, small, and very little is known about the basic elemental steps governing the photo-catalyzed chemical reactions on TiO_2. The literature presented in this review concludes that STM is a very valuable technique for studying the model system relevant to heterogeneous catalysis and photo-catalysis. However, the technique has its limitations due to the requirement of the model surface, in addition, the sample has to be extremely clean. Therefore, suitable samples fit the standards of STM scanning are difficult to prepare. In most cases, researchers have to rely on a chemical company, where a specimen with a single crystal surface is costly and time-consuming. Since many materials cannot be made in the form of a single crystal surface, therefore, the types of sample available are very few in number. If researchers come up with an idea of scanning on novel materials, then their first job would be to prepare a scanning-possible sample, which could be a challenge. There is a material gap between real catalysts applied in the industry and model catalysts applied in surface science. The pre-treatment of the samples inside the ultra-high pressure chamber could be tricky in case of pollution and a need to reconstruct. For example, for rutile TiO_2(110), a sputter with Ar^+ bombardment and annealing high up to 800 °C are necessary in order to make the surface conductive. The application of a high-pressure STM can solve the problem, which demands a better signal-to-noise ratio, and the recent success of utilizing Q-plus sensor with super-sensitivity in AFM promote the field of mechanism characterization toward a more precise direction [72–74]. With Q-plus sensor's ability in imaging a chemical bond with high resolution, it is fair to predict the mechanism of the photo-catalytic pathway. Also, in operation, the STM technique must combine with other techniques, such as TPD, photoemission spectroscopy (PES), and DFT, to gain more insights on a catalytic process. STM can provide on-site atomic information whereas TPD and PES work as composition characterization tool, and DFT can confirm a catalytic pathway by simulating the relevant process. In the near future, we are optimistic that by using STM, more insights into photo-catalyzed reactions on TiO_2 model surfaces, comprising both rutile and anatase surfaces can be obtained.

Table 1. Common traits in the behavior of adsorption, diffusion and photocatalytic reaction.

Organic Molecule	Adsorption	Diffusion	Photocatalytic Reaction
Alcohols	(1) Molecular adsorption at 5f-Ti (2) Dissociative adsorption at O_{vac}	(1) Diffusion along the Ti rows (2) Diffusion perpendicular to Ti rows mediated by H adatom	(1) Aldehyde formation with Ti-bound adsorbates (2) Carboxylate in O_{vac}-bound adsorbates
Carboxylic acids	(1) Carboxylate species with deprotonation in bidentate bonding to two 5f-Ti sites	(1) TMA barely diffuse (2) Physisorbed TMAA diffuse along Ti rows	(1) CO_2 and tert-butyl radical with Ti-bound adsorbates (2) Stability with O_{vac}-bound species
Aromatic compounds	(1) Easy to form ordered overlayer (2) Aromatic ring controls the geometry of adsorbates	(1) Adsorbate-substrate interaction (2) Coverage are determining factors	(1) No aromatic ring opening

Author Contributions: Conceptualization, P.H. and B.L.; methodology, P.H.; investigation, P.H.; resources, P.H. and B.L.; data curation, P.H.; writing—original draft preparation, P.H.; writing—review and editing, P.H., P.K. and B.L.; supervision, B.L.; project administration, B.L.; funding acquisition, P.H. and B.L.

Funding: This research was funded by "A Project of Shandong Province Higher Educational Science and Technology Program, grant number J18KB098".

Conflicts of Interest: The authors declare no conflict of interest. The funders had no role in the design of the study; in the collection, analyses, or interpretation of data; in the writing of the manuscript, or in the decision to publish the results.

References

1. Fujishima, A.; Honda, K. Electrochemical photolysis of water at a semiconductor electrode. *Nature* **1972**, *238*, 37–38. [CrossRef] [PubMed]
2. Hashimoto, K.; Irie, H.; Fujishima, A. TiO_2 photocatalysis: A historical overview and future prospects. *Jpn. J. Appl. Phys.* **2005**, *44*, 8269–8285. [CrossRef]
3. Baba, R.; Konda, R.; Fujishima, A.; Honda, K. Photoelectrochemical deposition of metals on TiO_2 powders in the presence of alcohols. *Chem. Lett.* **1986**, *15*, 1307–1310. [CrossRef]
4. Wang, R.; Hashimoto, K.; Fujishima, A.; Chikuni, M.; Kojima, E.; Kitamura, A.; Shimohigoshi, M.; Watanabe, T. Light-induced amphiphilic surfaces. *Nature* **1997**, *388*, 431–432. [CrossRef]
5. Nakabayashi, S.; Fujishima, A.; Honda, K. Single charge accumulation dynamics on photocatalytic TiO_2 particles in ethanol slurries by time domain reflectometry. *J. Am. Chem. Soc.* **1985**, *107*, 250–251. [CrossRef]
6. O'Regan, B.; Grätzel, M. A low-cost, high-efficiency solar cell based on dye-sensitized colloidal TiO_2 films. *Nature* **1991**, *353*, 737–740. [CrossRef]
7. Bahnemann, W.; Muneer, M.; Haque, M.M. Titanium dioxide-mediated photocatalysed degradation of few selected organic pollutants in aqueous suspensions. *Catal. Today* **2007**, *124*, 133–148. [CrossRef]
8. Sunada, K.; Watanabe, T.; Hashimoto, K. Studies on photokilling of bacteria on TiO_2 thin film. *J. Photochem. Photobiol. A Chem.* **2003**, *156*, 227–233. [CrossRef]
9. Li, F.B.; Li, X.Z.; Hou, M.F. Photocatalytic degradation of 2-mercaptobenzothiazole in aqueous La^{3+}-TiO_2 suspension for odor control. *Appl. Catal. B Environ.* **2004**, *48*, 185–194. [CrossRef]
10. Imagawa, H.; Tanaka, T.; Takahashim, N.; Matsunaga, S.; Suda, A.; Shinjoh, H. Synthesis and characterization of Al_2Ow and ZrO_2-TiO_2 nano-composite as a support for NOx storage-reduction catalyst. *J. Catal.* **2007**, *251*, 315–320. [CrossRef]
11. Mills, A.; Davies, R.H.; Worsley, D. Water purification by semiconductor photocatalysis. *Chem. Soc. Rev.* **1993**, *22*, 417–425. [CrossRef]

12. Hoffmann, M.R.; Martin, S.T.; Choi, W.; Bahnemann, D.W. Environmental applications of semiconductor photocatalysis. *Chem. Rev.* **1995**, *95*, 69–96. [CrossRef]
13. Kamat, P.V. Photophysical, photochemical and photocatalytic aspects of metal nanoparticles. *J. Phys. Chem. C* **2002**, *106*, 7729–7744. [CrossRef]
14. Carp, O.; Huisman, C.L.; Reller, A. Photoinduced reactivity of titanium dioxide. *Prog. Solid State Chem.* **2004**, *32*, 33–177. [CrossRef]
15. Fujishima, A.; Zhang, X.; Tryk, D.A. TiO_2 photocatalysis and related surface phenomena. *Surf. Sci. Rep.* **2008**, *63*, 515–582. [CrossRef]
16. Karunagaran, B.; Uthirakumar, P.; Chung, S.J.; Velumani, S.; Suh, E.K. TiO_2, thin film gas sensor for monitoring ammonia. *Mater. Charact.* **2007**, *58*, 680–684. [CrossRef]
17. Hu, L.H.; Dai, S.Y.; Weng, J.; Xiao, S.F.; Sui, Y.F.; Huang, Y.; Chen, S.H.; Kong, F.T.; Pan, X.; Liang, L.Y.; Wang, K.J. Microstructure design of nanoporous TiO_2 photoelectrodes for dye-sensitized solar cell modules. *J. Phys. Chem. B* **2007**, *111*, 358–362. [CrossRef]
18. Hong, S.P.; Park, J.; Bhat, S.S.M.; Lee, T.H.; Lee, S.A.; Hong, K.; Choi, M.J.; Shokouhimehr, M.; Jang, H.W. Comprehensive study on the morphology control of TiO_2 nanorods on foreigh substrates by the hydrothermal method. *Cryst. Growth Des.* **2018**, *18*, 6504–6512. [CrossRef]
19. Schubert, G.; Bánsági, T.; Solymosi, F. Photocatalytic decomposition of methyl formate over-supported Pt metals. *J. Phys. Chem. C* **2013**, *117*, 22797–22804. [CrossRef]
20. Neatu, S.; Maciá-Agulló, J.A.; Concepción, P.; Garcia, H. Gold-copper nanoalloys supported on TiO_2 as photocatalysts for CO_2 reduction by water. *J. Am. Chem. Soc.* **2014**, *136*, 15969–15976. [CrossRef]
21. Cong, Y.; Zhang, J.L.; Chen, F.; Anpo, M.; He, D.N. Preparation, photocatalytic activity, and mechanism of nano-TiO_2 co-doped with nitrogen and iron (III). *J. Phys. Chem. C* **2007**, *111*, 10618–10623. [CrossRef]
22. Jia, Y.N.; Zhan, S.H.; Ma, S.L.; Zhou, Q.X. Fabrication of TiO_2-Bi_2WO_6 binanosheet for enhanced solar photocatalytic disinfection of *E. coli*: Insights on the mechanism. *ACS Appl. Mater. Interfaces* **2016**, *8*, 6841–6851. [CrossRef] [PubMed]
23. Boschloo, G.K.; Goossens, A. Electron trapping in porphyrin-sensitized porous nanocrystalline TiO_2 electrodes. *J. Phys. Chem.* **1996**, *100*, 19489–19494. [CrossRef]
24. Wang, X.L.; Feng, Z.C.; Shi, J.Y.; Jia, G.Q.; Shen, S.; Zhou, J.; Li, C. Trap states and carrier dynamics of TiO_2 studied by photoluminescence spectroscopy under weak excitation condition. *Phys. Chem. Chem. Phys.* **2012**, *12*, 7083–7090. [CrossRef]
25. Leytner, S.; Hupp, J.T. Evaluation of the energetics of electron trap states at the nanocrystalline titanium dioxide/aqueous solution interface via time-resolved photoacoustic spectroscopy. *Chem. Phys. Lett.* **2000**, *330*, 231–236. [CrossRef]
26. Schneider, J.; Matsuoka, M.; Takeuchi, M.; Zhang, J.L.; Horiuchi, Y.; Anpo, M.; Bahnemann, D.W. Understanding TiO_2 photocatalysis: Mechanisms and materials. *Chem. Rev.* **2014**, *114*, 9919–9986. [CrossRef] [PubMed]
27. Wendt, S.; Sprunger, P.T.; Lira, E.; Madsen, G.K.H.; Li, Z.; Hansen, J.Ø.; Mattuesen, J.; Blekinge-Rasmussen, A.; Lægsgaard, E.; Hammer, B.; et al. The role of interstitial sites in the Ti_{3d} defect state in the band gap of titania. *Science* **2008**, *320*, 1755–1759. [CrossRef] [PubMed]
28. Sasahara, A.; Pang, C.L.; Onishi, H. STM observation of a ruthenium dye adsorbed on a TiO_2(110) surface. *J. Phys. Chem. B* **2006**, *110*, 4751–4755. [CrossRef]
29. Li, S.C.; Diebold, U. Reactivity of TiO_2 rutile and anatase toward nitroaromatics. *J. Am. Chem. Soc.* **2009**, *132*, 64–66. [CrossRef]
30. Potapenko, D.V.; Li, Z.; Osgood, R.M. Dissociation of single 2-chloroanthracene molecules by STM-tip electron injection. *J. Phys. Chem. C* **2012**, *116*, 4679–4685. [CrossRef]
31. Hansen, J.Ø.; Mattiesen, J.; Lira, E.; Lammich, L.; Wendt, S. A new recipe for preparing oxidized TiO_2(110) surfaces: An STM study. *Surf. Sci.* **2017**, *666*, 113–122. [CrossRef]
32. Lira, E.; Huo, P.P.; Hansen, J.Ø.; Rieboldt, F.; Bechstein, R.; Wei, Y.Y.; Streber, R.; Porsgaard, S.; Li, Z.S.; Lægsgaard, E.; et al. Effects of the crystal reduction state on the interaction of oxygen with rutile TiO_2(110). *Catal. Today* **2012**, *182*, 25–38. [CrossRef]
33. Henderson, M.A.; White, J.M.; Uetsuka, H.; Onishi, H. Selectivity changes during organic photooxidation on TiO_2 role of O_2 pressure and organic coverage. *J. Catal.* **2006**, *238*, 153–164. [CrossRef]

34. Yang, F.; Chen, M.S.; Goodman, D.W. Sintering of Au particles supported on TiO_2(110) during CO oxidation. *J. Phys. Chem. C* **2009**, *113*, 254–260. [CrossRef]
35. Hansen, J.Ø.; Huo, P.P.; Martinez, U.; Lira, E.; Wei, Y.Y.; Streber, R.; Lægsgaard, E.; Hammer, B.; Wendt, S.; Besenbacher, F. Direct evidence for ethanol dissociation on rutile TiO_2(110). *Phys. Rev. Lett.* **2011**, *107*, 136102. [CrossRef] [PubMed]
36. Muller, K.; Lu, D.; Senanayake, S.D.; Starr, D.E. Monoethanolamine adsorption on TiO_2(110): Bonding, structure, and implications for use as a model solid-supported CO_2 capture material. *J. Phys. Chem. C* **2014**, *118*, 1576–1586. [CrossRef]
37. Zhang, Z.; Bondarchuk, O.; White, J.M.; Kay, B.D.; Dohnálek, Z. Imaging adsorbate O–H bond cleavage: Methanol on TiO_2(110). *J. Am. Chem. Soc.* **2006**, *128*, 4198–4199. [CrossRef]
38. Grätzel, M. Photoelectrochemical cells. *Nature* **2001**, *414*, 338–344. [CrossRef]
39. Lyubinetsky, I.; Yu, Z.Q.; Henderson, M.A. Direct observation of adsorption evolution and bonding configuration of TMAA on TiO_2(110). *J. Phys. Chem. C* **2007**, *111*, 4342–4346. [CrossRef]
40. Lyubinetsky, I.; Deskins, N.A.; Du, Y.; Vestergaard, E.K.; Kim, D.J.; Dupuis, M. Adsorption state and mobility of trimethylacetic acid molecules on reduced TiO_2(110) surface. *Phys. Chem. Chem. Phys.* **2010**, *12*, 5986–5992. [CrossRef]
41. Grinter, D.C.; Woolcot, T.; Pang, C.L.; Thornton, G. Ordered carboxylates on TiO_2(110) formed at aqueous interfaces. *J. Phys. Chem. Lett.* **2014**, *5*, 4265–4269. [CrossRef] [PubMed]
42. Tanner, R.E.; Sasahara, A.; Liang, Y.; Altman, E.I.; Onishi, H. Formic acid adsorption on anatase TiO_2(001)-(1×4) thin films studied by NC-AFM and STM. *J. Phys. Chem. B* **2002**, *106*, 8211–8222. [CrossRef]
43. Grinter, D.C.; Nicotra, M.; Thornton, G. Acetic acid adsorption on anatase TiO_2(101). *J. Phys. Chem. C* **2012**, *116*, 11643–11651. [CrossRef]
44. Pang, C.L.; Watkins, M.; Cabailh, G.; Ferrero, S.; Ngo, L.T.; Chen, Q.; Humphrey, D.S.; Shluger, A.L.; Thornton, G. Bonding of methyl phosphonate to TiO_2(110). *J. Phys. Chem. C* **2010**, *114*, 16983–16988. [CrossRef]
45. Guo, Q.; Cocks, I.; Williams, E.M. The adsorption of benzoic acid on a TiO_2 (110) surface studied using STM, ESDIAD and LEED. *Surf. Sci.* **1997**, *393*, 1–11. [CrossRef]
46. Prauzner-Bechcicki, J.S.; Godlewski, S.; Tekiel, A.; Cyganik, P.; Budzioch, J.; Szymonski, M. High-resolution STM studies of terephthalic acid molecules on rutile TiO_2(110)-(1 × 1) surfaces. *J. Phys. Chem. C* **2009**, *113*, 9309–9315. [CrossRef]
47. Tekiel, A.; Prauzner-Bechcicki, J.S.; Godlewski, S.; Budzioch, J.; Szymonski, M. Self-assembly of terephthalic acid on rutile TiO_2(110): Toward chemically functionalized metal oxide surfaces. *J. Phys. Chem. C* **2008**, *112*, 12606–12609. [CrossRef]
48. Suzuki, S.; Yamaguchi, Y.; Onishi, H.; Sasaki, T.; Fukui, K.I.; Iwasawa, Y. Study of pyridine and its derivatives adsorbed on a TiO_2(110)-(1×1) surface by means of STM, TDS, XPS and MD calculation in relation to surface acid-base interaction. *J. Chem. Soc. Faraday Trans.* **1998**, *94*, 161–166. [CrossRef]
49. Otero-Irurueta, G.; Martínez, J.I.; Lovat, G.; Lanzilotto, V.; Méndez, J.; López, M.F.; Floreano, L.; Martín-Gago, J.A. Densely packed perylene layers on the rutile TiO_2(110)-(1 × 1) surface. *J. Phys. Chem. C* **2015**, *119*, 7809–7816. [CrossRef]
50. Lanzilotto, V.; Lovat, G.; Otero, G.; Sanchez, L.; López, M.F.; Méndez, J.; Martín-Gago, J.A.; Bavdek, G.; Floreano, L. Commensurate growth of densely packed PTCDI islands on the rutile TiO_2(110) surface. *J. Phys. Chem. C* **2013**, *117*, 12639–12647. [CrossRef]
51. Potapenko, D.V.; Choi, N.J.; Osgood, R.M. Adsorption geometry of anthracene and 4-bromobiphenyl on TiO_2(110) surfaces. *J. Phys. Chem. C* **2010**, *114*, 19419–19424. [CrossRef]
52. Wang, Y.; Ye, Y.; Wu, K. Adsorption and assembly of copper phthalocyanine on cross-linked TiO_2(110)-(1×2) and TiO_2(210). *J. Phys. Chem. B* **2006**, *110*, 17960–17965. [CrossRef] [PubMed]
53. Feng, H.; Liu, L.; Dong, S.; Cui, X.; Zhao, J.; Wang, B. Dynamic processes of formaldehyde at terminal Ti sites on the rutile TiO_2(110) surface. *J. Phys. Chem. C* **2016**, *120*, 24287–24293. [CrossRef]
54. Huo, P.P.; Hansen, J.Ø.; Martinez, U.; Lira, E.; Streber, R.; Wei, Y.; Lægsgaard, E.; Hammer, B.; Wendt, S.; Besenbacher, F. Ethanol diffusion on rutile TiO_2(110) mediated by H adatoms. *J. Phys. Chem. Lett.* **2012**, *3*, 283–288. [CrossRef] [PubMed]

55. Zhu, K.; Xia, Y.; Tang, M.; Wang, Z.T.; Lyubinetsky, I.; Ge, Q.; Dohnálek, Z.; Park, K.T.; Zhang, Z. Low-temperature reductive coupling of formaldehyde on rutile TiO_2(110). *J. Phys. Chem. C* **2015**, *119*, 18452–18457. [CrossRef]
56. Zhu, K.; Xia, Y.; Zhang, Z.; Park, K. Probing structure of cross-linked (1 × 2) rutile TiO_2(110): Adsorption of trimethyl acetic acid. *J. Phys. Chem. C* **2016**, *120*, 15257–15264. [CrossRef]
57. Jensen, S.C.; Shank, A.; Madix, R.J.; Friend, C.M. Butyrophenone on O-TiO_2(110): One-dimensional motion in a weakly confined potential well. *ACS Nano* **2012**, *6*, 2925–2930. [CrossRef]
58. Hansen, J.Ø.; Bebensee, R.; Martinez, U.; Porsgaard, S.; Lira, E.; Wei, Y.Y.; Lammich, L.; Li, Z.S.; Idriss, H.; Besenbacher, F.; et al. Unravelling site-specific photo-reactions of ethanol on rutile TiO_2(110). *Sci. Rep.* **2006**, *6*, 21990. [CrossRef]
59. Katsiev, K.; Harrison, G.; Alghamdi, H.; Alsalik, Y.; Wilson, A.; Thornton, G.; Idriss, H. Mechanism of ethanol photooxidation on single-crystal anatase TiO_2(101). *J. Phys. Chem. C* **2017**, *121*, 2940–2950. [CrossRef]
60. Zhou, C.; Ren, Z.; Tan, S.; Ma, Z.; Mao, X.; Dai, D.; Fan, H.; Yang, X.; LaRue, J.; Cooper, R.; et al. Site-specific photocatalytic splitting of methanol on TiO_2(110). *Chem. Sci.* **2010**, *1*, 575–580. [CrossRef]
61. Wei, D.; Jin, X.; Huang, C.; Dai, D.; Ma, Z.; Li, W.X.; Yang, X. Direct imaging single methanol molecule photocatalysis on titania. *J. Phys. Chem. C* **2015**, *119*, 17748–17754. [CrossRef]
62. Phillips, K.R.; Jensen, S.C.; Baron, M.; Li, S.C.; Friend, C.M. Sequential photo-oxidation of methanol to methyl formate on TiO_2(110). *J. Am. Chem. Soc.* **2013**, *135*, 574–577. [CrossRef] [PubMed]
63. Setvin, M.; Shi, X.; Hulva, J.; Simschitz, T.; Parkinson, G.S.; Schmid, M.; Valentin, C.D.; Selloni, A.; Diebold, U. Methanol on anatase TiO_2(101): Mechanistic insights into photocatalysis. *ACS Catal.* **2017**, *7*, 7081–7091. [CrossRef] [PubMed]
64. Ariga, H.; Taniike, T.; Morikawa, H.; Tada, M.; Min, B.K.; Watanabe, K.; Watanabe, Y.; Ikeda, S.; Saiki, K.; Iwasawa, Y. Surface-mediated visible-light photo-oxidation on pure TiO_2(001). *J. Am. Chem. Soc.* **2009**, *2*, 14670–14672. [CrossRef] [PubMed]
65. Henderson, M.A.; Epling, W.S.; Peden, C.H.F.; Perkins, C.L. Insights into photoexcited electron scavenging processes on TiO_2 obtained from studies of the reaction of O_2 with OH groups adsorbed at electronic defects on TiO_2(110). *J. Phys. Chem. B* **2003**, *107*, 534–545. [CrossRef]
66. White, J.M.; Henderson, M.A. Trimethyl acetate on TiO_2(110): Preparation and anaerobic photolysis. *J. Phys. Chem. B* **2005**, *109*, 12417–12430. [CrossRef] [PubMed]
67. Wang, Z.T.; Deskins, N.A.; Henderson, M.A.; Lyubinetsky, I. Inhibitive influence of oxygen vacancies for photoactivity on TiO_2(110). *Phys. Rev. Lett.* **2012**, *109*, 266103. [CrossRef]
68. Wang, Z.T.; Henderson, M.A.; Lyubinetsky, I. Origin of coverage dependence in photoreactivity of carboxylate on TiO_2(110): Hindering by charged coadsorbed hydroxyls. *ACS Catal.* **2015**, *5*, 6463–6467. [CrossRef]
69. Denis, V. Potapenko, photoreactions on a single isolated TiO_2 nanocrystal on Au(111): Photodecomposition of TMAA. *J. Phys. Chem. C* **2015**, *119*, 28946–28953. [CrossRef]
70. Landis, E.C.; Jensen, S.C.; Phillips, K.R.; Friend, C.M. Photostability and thermal decomposition of benzoic acid on TiO_2. *J. Phys. Chem. C* **2012**, *116*, 21508–21513. [CrossRef]
71. Jensen, S.C.; Phillips, K.R.; Baron, M.; Landis, E.C.; Friend, C.M. Norrish type I surface photochemistry for butyrophenone on TiO_2(110). *Phys. Chem. Chem. Phys.* **2013**, *15*, 5193–5201. [CrossRef] [PubMed]
72. Zhang, J.; Chen, P.; Yuan, B.; Ji, W.; Cheng, Z.; Qiu, X. Real-space identification of intermolecular bonding with atomic force microscopy. *Science* **2013**, *342*, 611–614. [CrossRef] [PubMed]
73. Peng, J.; Guo, J.; Hapala, P.; Cao, D.; Ma, R.; Cheng, B.; Xu, L.; Ondráček, M.; Jelínek, P.; Wang, E.; et al. Weakly perturbative imaging of interfacial water with submolecular resolution by atomic force microscopy. *Nat. Commun.* **2018**, *9*, 122. [CrossRef] [PubMed]
74. Guo, J.; Meng, X.; Chen, J.; Peng, J.; Sheng, J.; Li, X.Z.; Xu, L.; Shi, J.R.; Wang, E.; Jiang, Y. Real-space imaging of interfacial water with submolecular resolution. *Nat. Mater.* **2014**, *5*, 184–189. [CrossRef] [PubMed]